Clinical system for interstitial photodynamic therapy with combined on-line dosimetry measurements

Soto Thompson, Marcelo; Johansson, Ann; Johansson, Thomas; Andersson-Engels, Stefan; Svanberg, Sune; Bendsöe, Niels; Svanberg, Katarina

Published in:
Applied Optics

2005

Clinical system for interstitial photodynamic therapy with combined on-line dosimetry measurements

Marcelo Soto Thompson, Ann Johansson, Thomas Johansson, Stefan Andersson-Engels, Sune Svanberg, Niels Bendsoe, and Katarina Svanberg

A system for interstitial photodynamic therapy with δ-aminolaevulinic acid and multiple optical fibers has been developed. The system enables photodynamic treatment of large embedded tumor volumes and utilizes real-time measurements to allow on-line dosimetry. Important parameters such as light fluence rate, sensitizer fluorescence intensity, and changes in local blood oxygen saturation are measured with the same fibers that deliver the therapeutic light. Data from the first clinical treatments on nodular basal cell carcinomas indicate a major treatment-induced light absorption increase, rapid sensitizer photobleaching, and a relatively constant global tissue oxygen saturation level during the treatment. © 2005 Optical Society of America

OCIS codes: 170.5180, 120.389, 170.6510, 170.1460.

1. Introduction

As malignant diseases continue to plague humanity, much effort is put into trying to develop new and better treatment modalities. One such method is photodynamic therapy (PDT).[1–3] PDT relies on the application of a photosensitizer (or its precursor) followed by the activation of the photosensitizer with light. The activated sensitizer will react with the oxygen present in the tissue forming highly toxic radicals and will induce tissue necrosis or apoptosis. Since most photosensitizers will accumulate to a higher extent in malignant tissue than in healthy tissue, the treatment targets the malignancies while sparing the surrounding healthy tissue. The introduction of δ-aminolaevulinic acid (ALA) as a sensitizer precursor, inducing protoporphyrin IX (PpIX) as a sensitizing agent, has led to a substantial increase in the clinical acceptance of the method, especially for some types of skin lesion where ALA PDT now can be considered the treatment of choice.[4–9]

Use of PDT is usually considered to be limited to thin (<3 mm) superficial lesions or lesions accessible through body cavities. Thus, in an effort to extend the possible indications for PDT, we present a system for interstitial PDT (IPDT), where thick or embedded tumors are treated using optical fibers inserted into the tumor. IPDT has been pursued for many indications, for example, prostate,[10] liver,[11] and pancreatic cancer[12]; and in this clinical or preclinical work it has been stated that the main drawbacks of the method as applied today are the limited light penetration and the lack of a more precise light dosimetry. A special aspect of the work performed in our group is to use the optical fibers not only to deliver the therapeutic light but also to perform optical measurements to assess parameters of therapeutic interest and to monitor the treatment progression. Examples of such parameters are tissue oxygenation, light fluence rate, and sensitizer fluorescence. The basic concept has been previously described in more detail elsewhere[13] and is schematically shown in Fig. 1. The development of this concept has been pursued in incremental steps[14,15] with promising experimental[16] and clinical results.[17]

In the previous system[14] it was possible to measure the therapeutic light flux in the lesion but the system

When this research was performed, M. Soto Thompson (marcelo@fysik.lth.se), A. Johansson, T. Johansson, S. Andersson-Engels, and S. Svanberg were with the Department of Physics, Lund Institute of Technology, P.O. Box 118, SE-221 00 Lund, Sweden. T. Johansson is now with SpectraCare AB, Ideon Research Park, Ole Römers väg 16, SE-223 70 Lund, Sweden. N. Bendsoe is with the Department of Dermatology and Venereology, Lund University Hospital, SE-221 85 Lund, Sweden, and the Lund University Medical Center Laser Centre, P.O. Box 118, SE-221 00 Lund, Sweden. K. Svanberg is with the Department of Oncology, Lund University Hospital, SE-221 85 Lund, Sweden, and the Lund University Medical Laser Centre, P.O. Box 118, SE-221 00 Lund, Sweden.

Received 20 July 2004; revised manuscript received 14 February 2005; accepted 20 February 2005.

0003-6935/05/194023-09$15.00/0

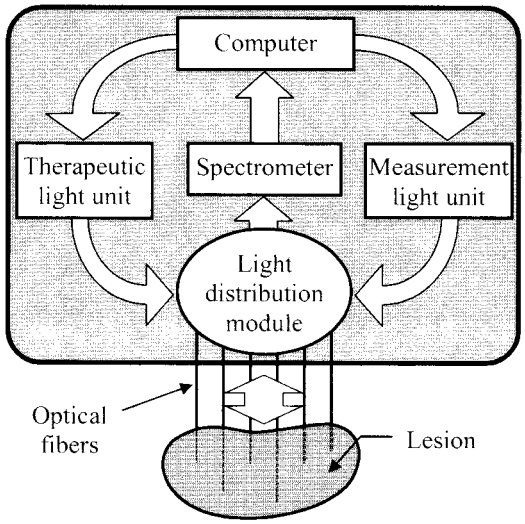

Fig. 1. Schematic diagram of an interactive system for IPDT.

construction did not allow the measurements of other parameters. The sensitizer fluorescence was in that case assessed by using a separate fluorosensor[18,19] with a separate measurement fiber. The novel approach[20] reported in the present paper enables us to perform light flux as well as sensitizer fluorescence and oxygenation monitoring through the same fibers that deliver the therapeutic light.

In Section 2 the construction of the new interactive system is described, followed by a presentation of the implementation of the dosimetry calculations and the measurements of therapeutic interest. Finally, results from the first clinical application of the new system are presented, and future development toward a fully interactive system for IPDT is discussed.

2. System Description

A. Hardware Overview

The equipment is controlled by a laptop computer with a custom-made program based on LabVIEW (National Instruments, Austin, Texas). As shown in Fig. 1, the central part of the system consists of a light distribution module that determines whether the system is running in therapeutic mode or measurement mode. The system (except the computer) is enclosed in a clinically compatible case measuring 30 cm × 43 cm × 21 cm (length × width × height) and weighing 12 kg (see Fig. 2).

The light distribution module consists of two metal disks positioned at close proximity on a common axis (see Fig. 3). One of the disks can be rotated on the axis and has six fiber ports hexagonally placed at a fixed distance from the axis. These fiber ports have connectors where the patient fibers are attached. The fixed disk has a similar set of fiber ports, with the therapeutic light sources attached, facing the ports on the turnable disk. During the therapeutic mode, the light from the fiber-coupled light sources can be directly transmitted through the light distribution module into the patient fibers in a highly efficient way. The maximum therapeutic output power distributed on the six patient fibers is approximately 1.2 W. These fibers have a core diameter of 400 μm, a numerical aperture of 0.22, and an outer diameter of 0.88 mm. Before each treatment session, the patient fibers are calibrated to emit equal output powers while in therapeutic mode.

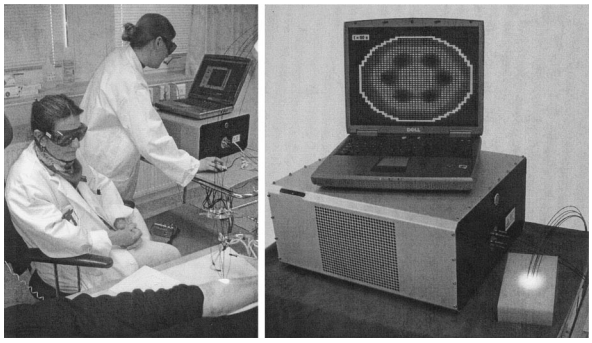

Fig. 2. System as seen in a clinical treatment situation and system overview during calibration.

For the measurement mode the turnable disk is rotated 30 deg. The fiber ports on the turnable disk now face another similar set of fiber ports on the fixed disk. Now the light distribution module serially couples one of up to three measurement light sources (in our case two) into one of the patient fibers, as shown in Fig. 4. These light sources are selected with a coupling unit that can be of a similar construction as the main light distribution module. The two light sources used are a diode laser at 635 nm and a light-emitting diode covering the wavelength interval from 750 to 800 nm. The third light source (not implemented) might, for example, be a violet diode laser emitting light at 405 nm to monitor the PpIX fluorescence before the therapeutic irradiation starts, which would enable the possibility to interactively insert the fibers where the PpIX concentration is the highest. The mechanism behind the light distribution modules is stable enough to allow for accurate repositioning, which means that the output power in each of the six patient fibers while in diagnostic mode is

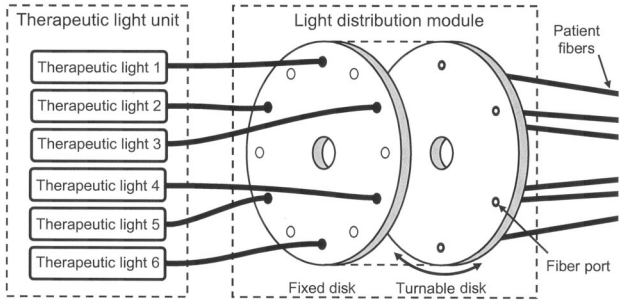

Fig. 3. Interactive IPDT system shown in the treatment mode. The disks in the light distribution module are placed in close proximity (here drawn apart) to each other on a common axis (not shown). The therapeutic light is coupled through the disks into the patient fibers. The components used in the measurement mode were omitted for clarity.

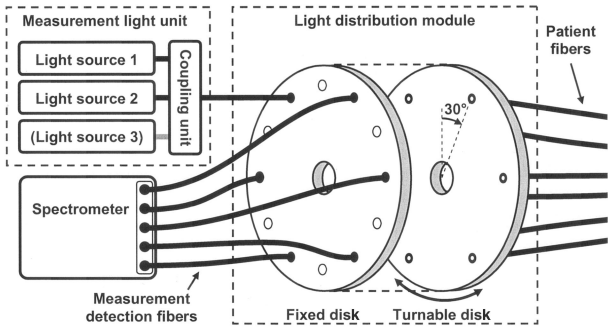

Fig. 4. Interactive IPDT system shown in the measurement mode, assessed by rotating the turnable light distributor disk 30 deg with respect to the disk position for treatment. Nonactive measurement light sources are shown in gray. The active light source is coupled into one patient fiber while the other five patient fibers collect the tissue response back into the spectrometer. By rotating the turnable disk in steps of 60 deg, all patient fibers can be made to act as transmitters for the individual light sources. The therapeutic components were omitted for clarity.

similar (±10%). The measurement light interacts with the tissue and is collected by the other five patient fibers. This light is guided back through the light distribution module that now redirects the light, by way of the measurement detection fibers, onto the entrance slit of an imaging spectrometer. The detection fibers are aligned linearly along the entrance slit of the spectrometer, and the collected light can therefore be resolved as five individual signals for each light source. After collecting a signal with sufficient signal-to-noise ratio from each light source, the light distribution module shifts the transmitting measurement fiber to each and every one of the patient fibers. The resulting number of data sets for every measurement session is 60 (2 light sources × 5 detection fibers × 6 excitation fibers). One full measurement session lasts for approximately 45 s.

B. Dosimetry Calculations

The fluence rate $\phi(\mathbf{r})$ in the treatment volume is determined by solving the steady-state diffusion equation[21]:

$$\nabla^2\phi(\mathbf{r}) - \mu_{\text{eff}}{}^2\phi(\mathbf{r}) = \sum_i S(\mathbf{r}_i), \tag{1}$$

where $\mu_{\text{eff}} = [3\mu_a(\mu_a + \mu_s')]^{1/2}$; here μ_a and μ_s' are the effective attenuation, absorption, and reduced scattering coefficients (see Table 1).[22] The source term $\Sigma S(\mathbf{r}_i)$ is modeled as isotropic point sources, denoted by the index i. In the case of superficial lesions, the extrapolated boundary condition is used to solve Eq. (1).[23] A commercial program (FEMLAB, Comsol, Sweden) is used to model the fluence rate distribution with the finite-element method. The tumor geometries are approximated with either ellipsoids or flat cylinders with an elliptical cross section. To give a fluence rate distribution within the tumor that is as homogeneous as possible, while sparing normal surrounding tissue, the fibers are placed in either one or two planes depending on the tumor thickness and at a distance from the tumor center of approximately 7/10 of the tumor radius. This distance has been determined by maximizing the fluence rate, as given by the analytical solution of the diffusion equation in an infinite homogeneous medium, at the boundary of an ellipsoid. On the basis of the fluence rate distribution, the absorbed dose throughout the tumor volume is calculated. With a threshold (15 J/cm^{-3}) for the absorbed light dose considered sufficient to induce cell necrosis, an estimate of the necessary treatment time is calculated.[14] This prediction is dependent on fiber positions, tissue optical properties, and choice of threshold for the absorbed light dose.

Table 1. Optical Parameters of Normal Tissue and Tumor Used

Tissue Type	μ_a (cm^{-1})	μ_s' (cm^{-1})
Normal	0.16	12.0
Tumor	0.31	12.4

C. Treatment Monitoring Measurements

As described above, the treatment is repeatedly interrupted to perform measurements to monitor the treatment. First, the fluence rate at 635 nm of the light emitted by each fiber is measured at the tip of all the other fibers. This measurement monitors the transmittance of the tissue during the treatment. Drastic changes in light transmission as a consequence of, e.g., blood coagulation or bleeding at the fiber tips can then be detected and an insufficient treatment may thus be prevented. The measurements make it also possible to compensate for treatment-induced variations in light transmission. Second, the sensitizer fluorescence at 705 nm induced by the measurement light source at 635 nm and its characteristic photobleaching are monitored during the treatment.[24] The final parameter measured is the oxygen saturation level S_{O_2} defined as

$$S_{O_2} = \frac{[HbO_2]}{[Hb] + [HbO_2]}, \tag{2}$$

with $[HbO_2]$ and [Hb] denoting the oxyhemoglobin and deoxyhemoglobin concentrations, respectively. Assuming that hemoglobin is the main absorbing tissue constituent, the absorption coefficients at 760 and 800 nm can be written as[25]

$$\mu_a^{760} \propto \varepsilon_{Hb}^{760}[Hb] + \varepsilon_{HbO_2}^{760}[HbO_2],$$

$$\mu_a^{800} \propto \varepsilon_{Hb}^{800}[Hb] + \varepsilon_{HbO_2}^{800}[HbO_2], \tag{3}$$

where ε_i^X is the extinction coefficient of species i at wavelength X. By utilizing Eqs. (2) and (3), the oxygen saturation can eventually be expressed as

$$S_{O_2} = \frac{1}{\varepsilon_{Hb}^{760} - \varepsilon_{HbO_2}^{760}} \left(\varepsilon_{Hb}^{760} - \varepsilon^{800} \frac{\mu_a^{760}}{\mu_a^{800}} \right), \quad (4)$$

utilizing that the extinction coefficients of Hb and HbO_2 are equal at the isobestic point at 800 nm.[25] Using the second diagnostic light source, the overall absorption can be monitored in the spectral interval between 750 and 800 nm. The fluence rate from the source fiber is approximated by the analytical solution to Eq. (1) for a point source in an infinite medium:

$$\phi(r) = \frac{P\mu_{eff}^{\ 2}}{4\pi\mu_a r} \exp(-\mu_{eff}^{\ r}), \quad (5)$$

where P is the power irradiated by the source fiber. By measuring the fluence rate with several detection fibers at different distances from the source fiber and fitting a curve to the measured values, μ_{eff} can be extracted both for 760 and 800 nm. Finally, by forming the ratio

$$\left(\frac{\mu_{eff}^{760}}{\mu_{eff}^{800}} \right)^2 = \frac{\mu_a^{760}(\mu_a^{760} + \mu_s'^{760})}{\mu_a^{800}(\mu_a^{800} + \mu_s'^{800})} \approx \frac{\mu_s'^{760}}{\mu_s'^{800}} \frac{\mu_a^{760}}{\mu_a^{800}}, \quad (6)$$

and inserting this into Eq. (4) we can calculate the oxygen saturation level. The last step in Eq. (6) is valid under the assumption that the reduced scattering coefficient is much larger than the absorption coefficient. The ratio of the reduced scattering coefficients can be calculated by assuming the following wavelength dependence of the tissue scattering[26]:

$$\mu_s' \propto \lambda^{-1.11}. \quad (7)$$

On the basis of the result of the latter measurement, a fractionized irradiation might be necessary to allow for an increased oxygen inflow to the treated region. The oxygenation data evaluation method is similar to the method used for a commercial product by Hamamatsu, C7473-36, in the sense that they both explore the absorption imprint of hemoglobin on the transmitted signal.

3. Patients

A total of ten treatments in eight patients were performed. The patients treated had histopathologically verified nodular basal cell carcinomas and were referred to the oncology clinic at the Lund University Hospital, Lund, Sweden. The clinical motivation of the study was to reduce the tumor volume prior to surgery or other conventional treatment. The study was performed with approval of the local ethics committee. At the time of treatment the tumor geometry was determined visually and by palpation by an experienced oncologist. The lesion was photosensitized by mixing ALA (MEDAC GmbH, Hamburg, Germany) into an oil-in-water emulsion (Essex Cream, Schering Corp., Kenilworth, New Jersey) to a concentration by weight of 20%, which was applied to the lesion 4–6 h before the therapeutic irradiation. The lesion was prepared according to clinical praxis by disinfecting the treatment area and subsequently administering Xylocain (AstraZeneca, Södertälje, Sweden) subcutaneously as anaesthetics. The sterilized fibers were inserted and subsequently fixed in a holder that in turn was attached to the patient stretcher.

4. Results

To show the capability of the instrument to measure parameters of therapeutic importance, typical data from an 80-year-old patient with a basil cell carcinoma are presented as a case study. The geometry of the lesion was found to be approximately cylindrical with a diameter of 14 mm and a depth of 3 mm. An output power of 75 mW for each of the six patient fibers resulted in an initial estimated treatment time of 400 s.

A. Light Fluence

In Fig. 5 the fluence rates at 635 nm as measured during the treatment are shown. To clearly resolve changes in the light transmission despite the different magnitudes of the detected signals from the various fibers, all signals were normalized to their respective initial value. In Fig. 5(a) treatment fiber 1 acts as the light transmitter and fibers 2–6 serve as detectors. In Figs. 5(b)–5(f) the light transmitter is fibers 2–6, respectively.

It can be seen that the light transmission between the fibers decreases during the treatment, and a similar trend was established during all but two treatment sessions. In some cases this transmission decrease is much more pronounced, as can be seen in fiber 3 in Fig. 5(f). This fiber was characterized by a significantly lowered transmission as compared with the other fibers during the entire treatment, although the magnitudes of the detected and transmitted signals were not significantly lower than the other transmission signals. This decrease could possibly be explained by either some local inhomogeneity, for example, a blood vessel, or that the distance between this fiber to the others was much larger than the distance between the other fibers. Hemorrhage at the fiber tip was not believed to cause this particular transmission decrease since blood pooling would have significantly decreased the magnitude of the transmission signal.

The six treatment lasers were turned off after 400 s at the predicted treatment time; however, the fluence rate, sensitizer fluorescence, and oxygenation measurements were carried out for another 320 s. According to, e.g., Fig. 5(b), some regions show a slight reversal of the treatment-induced absorption increase after the therapeutic irradiation has ended.

Assuming that the transmission changes are due to changes in tissue optical properties, the degree of transmission decrease depends on the interfiber distances. This is also reflected in Figs. 5(a)–5(f) where signals between fibers with the largest separations

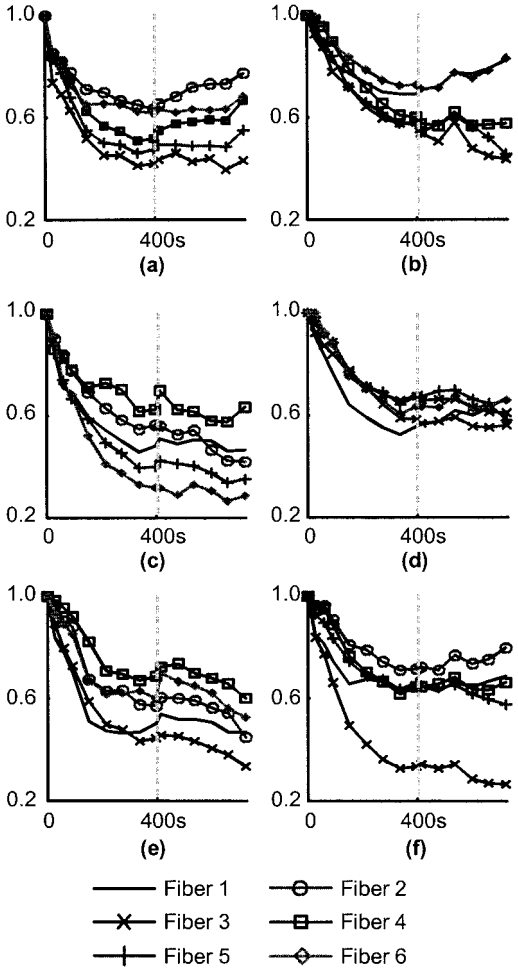

Fig. 5. Fluence rate at 635 nm as measured during the treatment. The time interval between measurement sequences was 30 s for the first 90 s of treatment; thereafter measurements were performed every minute up to an effective treatment time of 720 s. The end of the therapeutic irradiation is indicated by the dashed line.

show a more marked transmission decrease. If only including neighboring fibers, positioned in such a way that the interfiber distances are equal, the average transmission decrease was found to be 39% for this particular patient. A significant transmission decrease was found in seven of nine treatment sessions, where the significance was tested using a one-sided Student's t-test ($P < 0.02$). The average transmission decrease was 24% when taking into account data from nine treatment sessions, although an average decrease of 60% was found during one treatment session. Data from one of the treatment sessions were excluded from the analysis since the optical fibers lost their positions when the patient started coughing.

B. Sensitizer Fluorescence

The sensitizer fluorescence, induced with 635 nm light, measured at 705 nm as a function of the treatment time is shown in Fig. 6. The detected signals measured in each and every fiber were individually normalized to their respective initial value. Figure 6 shows the average of these normalized signals between neighboring fibers with the error bars denoting standard deviations (SDs). The reason for including only the fluorescence signal as measured in between nearby fibers is to obtain a photobleaching curve that is not influenced by the varying fiber separations. Note that the absorption increase as seen in Subsection 4.A was not compensated for when we plotted this average fluorescence signal.

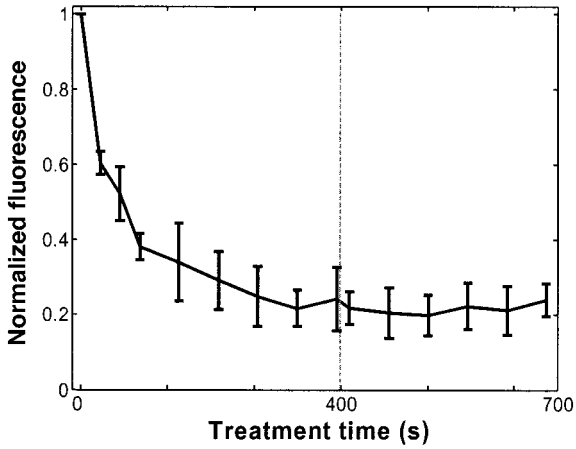

Fig. 6. Average of the normalized sensitizer fluorescence signal (±SD) at 705 nm during treatment. The therapeutic irradiation was turned off after 400 s, indicated by the dashed line.

The fluorescence level decreased to 22% of the initial signal for this particular treatment session, as compared with an average decrease to 15% of the initial level for the nine completed treatments.

C. Tissue Oxygenation

The final parameter monitored during the treatment is the local tissue oxygenation, and the average oxygen saturation level (±SD) during the treatment session is shown in Fig. 7. The vertical dashed line at 400 s indicates the time point when the therapeutic

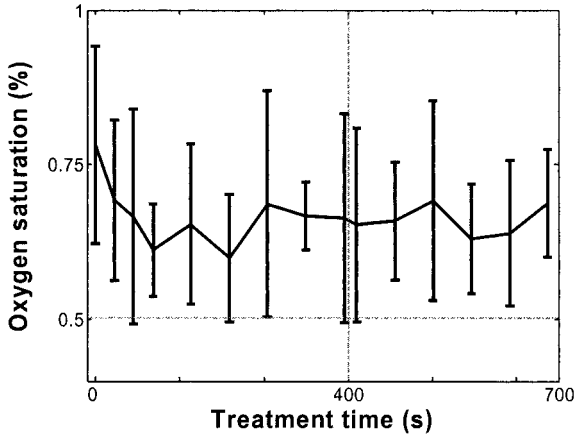

Fig. 7. Tissue oxygenation (±SD) as a function of the treatment time as measured during one treatment. The therapeutic irradiation was turned off after 400 s, indicated by the vertical dashed line. The horizontal dashed line indicates the 50% tissue oxygen saturation level.

irradiation was turned off, whereas the horizontal dashed line marks the 50% oxygen saturation level.

Data from all treatment sessions show that the average initial oxygen saturation level was 77% and no significant changes could be observed, apart from an indication of a small initial fast reduction, during the treatments. The significance level was tested using a Student's t-test at significance level $P = 0.01$. Lesions located in the face displayed slightly higher oxygenation levels than those located on the lower extremities, although these differences were not significant.

5. Discussion

PDT relies on the presence of three components: light, sensitizer, and oxygen; and in this study much effort has been put into monitoring these parameters in parallel to the treatment session to supervise and hopefully in the future be able to control the treatment progression. Here we describe the implementation of a system for IPDT using up to six treatment fibers for light delivery. The same fibers can be used for real-time monitoring of the fluence rate, the sensitizer fluorescence, and the tissue oxygenation allowing for on-line treatment supervision. In addition, by the monitoring of these parameters, possible correlations can be studied, which might add useful knowledge in the field of cancer treatment by means of PDT. One example of such a correlation is the higher rate of initial PpIX photobleaching in well-oxygenated tissue regions, a process that supports the idea of an oxygen dependence of the sensitizer bleaching.[27] Since a stable oxygen supply promotes an effective PDT treatment, other groups have proposed monitoring of the sensitizer fluorescence as a possible real-time treatment feedback.[24] Soumya and Foster have shown a 3- to 15-fold increase in light penetration at 630 nm when comparing a hypoxic to a well-oxygenated tissue phantom containing human erythrocytes, an effect that is explained by the stronger absorption of deoxyhemoglobin as compared to oxyhemoglobin at 630 nm.[28] This result implies that there is a strong connection between oxygen saturation level and tissue transmission. Conversely, a high fluence rate leads to oxygen depletion,[29] which in turn affects the photobleaching rate.

Addressing the fluence rate measurement, a significant absorption increase was found in seven of nine treatment sessions. Other groups have also reported on treatment-induced light transmission decrease in tissue during PDT. Chen *et al.* have observed 40%–80% reduction in fluence rate in normal canine prostate and give alterations of the local blood flow and perfusion as possible explanations.[30] Using an integrating sphere measurement setup, Nilsson *et al.* found a 60%–100% increase in the absorption coefficient after PDT of normal rat muscle sensitized with ALA-induced PpIX.[31] These authors argue that the increase in tissue absorption is due to damage to the tissue microcirculation. Other explanations include local hyperthermia, bleeding at the fiber tips,[32] and tissue deoxygenation as a consequence of the oxygen consumption by the photodynamical reaction.[28] Further evaluation of our data indicates that the light transmission changes are in fact due to tissue deoxygenation and changes in blood volume, and these results will be part of a future publication.[33]

The PDT-induced absorption increase causes the delivered light dose at the end of the treatment to fall below the calculated threshold dose and therefore prevents the peripheral tumor regions from being fully treated. On the basis of the dosimetric measurement, an interactive treatment could easily be implemented by prolonging the treatment time or increasing the fiber output power to compensate for the decreased light penetration. It should also be mentioned that, although the observed transmission decrease is present in all but two patients treated so far, the degree of transmission decrease varies on an interpatient basis. It is therefore necessary to monitor these changes during each individual treatment session and adjust the treatment parameters according to the measurement results.

Monitoring the sensitizer photobleaching is of course essential, since according to Robinson *et al.*[27] and Boere *et al.*[34] a strong correlation exists between the initial sensitizer photobleaching rate and the treatment outcome. This signal could be of importance for early-stage treatment feedback, but exactly how the treatment should be modified as a result of this information has to be studied in more detail. One should note that our indirect method of monitoring the tissue oxygen saturation assumes that there is a connection between the concentration of free oxygen molecules and the oxygenation level of the tissue.[35]

Results from all treatment sessions show no significant variations in tissue oxygen saturation, although a small initial decrease in oxygenation could be observed in all patients. The evaluation method of the near-infrared spectra is based on determining the effective absorption coefficient by means of spatially resolved spectroscopy and therefore relies on signals measured between all possible fiber combinations. This means that the light transmission is measured across the entire tumor geometry, which involves large source–detector separations and the signals can therefore be used only for determination of the global tissue oxygen saturation. Oxygen depletion is a local process and initially occurs close to the fiber tip, where the fluence rate is highest. Curnow *et al.*[36] and Woodhams *et al.*[37] have shown that, close to the source fiber, the photodynamic reaction induces a dramatic decrease of the oxygen saturation as measured either by means of tissue oxygen pressure (p_{O_2}) or visible light spectroscopy. When increasing the source–detector separation, this effect was less obvious and no changes were observable for source–detector separations of 3 mm or larger for continuous irradiation at 100 mW. Comparing continuous with fractionated irradiation, a significant decrease in oxygen saturation level was found only where the detection point fell within the area of necrosis. The authors speculate whether the light delivery conditions can be optimized based on real-time oxygen

monitoring, leading to improved treatment outcome. The herein proposed global method of data evaluation might explain the lack of significant changes in measured tissue oxygen saturation since data evaluation is based on source–detector separations of 5–8 mm. Possibly, the treatment time or fiber output power was not sufficient to induce necrosis in the entire interfiber volume. Furthermore, the large source–detector separation makes the method sensitive to tissue inhomogeneities. Data evaluation based on single fiber pairs gives a more local measure of the tissue oxygen saturation and will be part of a future publication.[33] The oxygen saturation level reported here, which might be described as an average over the entire tumor volume, is in agreement with oxygenation baseline levels reported on by others.[26] The lower limit for the tissue oxygenation for an effective treatment is an issue that has been debated in both PDT and radiotherapy.[7,38] Using the instrument reported here, this will be a question that we will address in future work.

The calculation of the tissue oxygenation level as well as the derivation of changes in tissue optical properties that are consistent with the light transmission changes depend on the exact positioning of the fibers. Knowledge of the exact fiber positions would avoid this source of error and make the data evaluation more stable. Ultrasound monitoring has a high enough spatial resolution to detect the optical fiber tips, and this mode of guiding and determining the fiber positions is already in use in IPDT of the prostate.[39,40] Ultrasound guidance during fiber insertion is therefore an attractive possibility for future treatment sessions.

The evaluation of the oxygen saturation signal assumes that deoxyhemoglobin and oxyhemoglobin are the only tissue constituents whose absorption might change during the treatment session. The observed absorption increase might be influenced by concentration changes of other tissue chromophores, such as water resulting from treatment-induced oedema.

The oxygen saturation signal can be used to monitor the possible need of a fractionated irradiation. Because of the introduction of the measurement sequences that interrupt the therapeutic irradiation, some irradiation fractionation with dark intervals of 45 s is already implemented. Fractionated irradiation enables some reperfusion of the treatment volume and has been shown to increase treatment response.[41] Therefore these signals are important for improvement of the treatment outcome. Future work includes implementing such therapeutic feedback based on real-time data analysis of the monitoring measurements to make the treatment truly interactive. Transmission changes, which might affect the tissue volume being treated, can easily be followed and compensated for by changing treatment time or fiber output power. When six patient fibers are used, the fluence rate measurements as exemplified in Fig. 5 result in 30 light transmission signals since five fibers are used to detect the transmitted light from one source fiber, and this procedure is repeated for all six patient fibers. This set of light transmission signals can also be used for low-resolution tomography of the flux in the tissue being treated.[42] Likewise the 30 fluorescence and 30 white-light penetration data sets will be used to construct a tomographic presentation of sensitizer and oxygen levels, respectively.

Using the light transmission signals between patient fibers, it is possible to calculate the tissue effective attenuation coefficient for each individual patient. In the future, this information could be used as input to the light distribution modeling performed prior to the therapeutic light delivery, resulting in a more accurate treatment time prediction.

For the possible use of other sensitizers, it is easy to replace the six therapeutic laser diodes with units of a suitable wavelength. Furthermore, by use of the option of a third diagnostic light source, flexibility for inducing fluorescence in a large variety of sensitizers is maintained.

6. Conclusion

We have reported on the construction of a system for IPDT of solid tumors, and the initial clinical results have been presented. Future work will involve implementing a full model for interactive treatment based on the real-time monitoring of fluence rate, sensitizer fluorescence, and blood oxygenation. Also, improving the fiber positioning system with ultrasound guidance, several other indications, for example, lesions in the gastrointestinal tract, lie within the foreseeable future of this system.

Sara Pålsson is greatly acknowledged for contributing to the scientific discussions. This research was supported by the Swedish Foundation for Strategic Research and in an earlier phase by VINNOVA. We are grateful to Epsilon Technology AB, and in particular to Anders Jeppsson for providing technical solutions and hardware integration. The Karolinska Development AB, Stockholm, and Lund University Developmental AB support the project economically through SpectraCure AB, which is set up to bring the research project into a powerful health care reality. The dedication of Thomas Andersson in this task is especially appreciated.

References

1. S. L. Marcus, "Photodynamic therapy of human cancer: clinical status, potential and needs," in *Future Directions and Applications in Photodynamic Therapy*, C. J. Gomer, ed., Vol. IS06 of the SPIE Institute Series (SPIE, 1990), pp. 5–56.
2. L. I. Grossweiner, *The Science of Phototherapy* (CRC Press, 1994).
3. T. J. Dougherty, C. J. Gomer, B. W. Henderson, G. Jori, D. Kessel, M. Korbelik, J. Moan, and Q. Peng, "Photodynamic therapy," J. Natl. Cancer Inst. **90,** 889–905 (1998).
4. J. C. Kennedy, R. H. Pottier, and D. C. Pross, "Photodynamic therapy with endogenous protoporphyrin IX: basic principles and present clinical experience," J. Photochem. Photobiol. B. **6,** 143–148 (1990).
5. J. C. Kennedy and R. H. Pottier, "Endogenous protoporphyrin IX, a clinically useful photosensitizer for photodynamic therapy," J. Photochem. Photobiol. B. **14,** 275–292 (1992).
6. K. Svanberg, T. Andersson, D. Killander, I. Wang, U. Stenram,

S. Andersson-Engels, R. Berg, J. Johansson, and S. Svanberg, "Photodynamic therapy of non-melanoma malignant tumours of the skin using topical δ-amino levulinic acid sensitization and laser irradiation," Br. J. Dermatol. **130,** 743–751 (1994).
7. Q. Peng, T. Warloe, K. Berg, J. Moan, M. Kongshaug, K.-E. Giercksky, and J. M. Nesland, "5-aminolevulinic acid-based photodynamic therapy: clinical research and future challenges," Cancer **79,** 2282–2308 (1997).
8. I. Wang, N. Bendsoe, C. af Klinteberg, A. M. K. Enejder, S. Andersson-Engels, S. Svanberg, and K. Svanberg, "Photodynamic therapy versus cryosurgery of basal cell carcinomas; results of a phase III randomized clinical trial," Br. J. Dermatol. **144,** 832–840 (2001).
9. K. A. Salva, "Photodynamic therapy: unapproved uses, dosages, or indications," Clin. Dermatol. **20,** 571–581 (2002).
10. S. C. Chang, G. Buonaccorsi, A. MacRobert, and S. G. Bown, "Interstitial and transurethral photodynamic therapy of the canine prostate using *meso-tetra*-(*m*-hydroxyphenyl) chlorin," Int. J. Cancer **67,** 555–562 (1996).
11. T. J. Vogl, K. Eichler, M. G. Mack, S. Zangos, C. Herzog, A. Thalhammer, and K. Engelmann, "Interstitial photodynamic laser therapy in interventional oncology," Eur. Radiol. **14,** 1063–1073 (2004).
12. S. G. Bown, A. Z. Rogowska, D. E. Whitelaw, W. R. Lees, L. B. Lovat, P. Ripley, L. Jones, P. Wyld, A. Gillams, and A. W. Hatfield, "Photodynamic therapy for cancer of the pancreas," Gut **50,** 549–557 (2002).
13. S. Svanberg, S. Andersson-Engels, R. Berg, J. Johansson, and K. Svanberg, "System for laser treatments of tumours," Swedish patent SE 950 1278 (6 October 1996).
14. T. Johansson, M. Soto Thompson, M. Stenberg, C. af Klinteberg, S. Andersson-Engels, S. Svanberg, and K. Svanberg, "Feasibility study of a novel system for combined light dosimetry and interstitial photodynamic treatment of massive tumors," Appl. Opt. **41,** 1462–1468 (2002).
15. S. Andersson-Engels, N. Bendsoe, A. Johansson, T. Johansson, S. Pålsson, M. Soto Thompson, K. Svanberg, and S. Svanberg, "Integrated system for interstitial photodynamic therapy," in *Therapeutic Laser Applications and Laser-Tissue Interactions*, R. Steiner, ed., Proc. SPIE **5142,** 42–48 (2003).
16. M. Stenberg, M. Soto Thompson, T. Johansson, S. Pålsson, C. af Klinteberg, S. Andersson-Engels, U. Stenram, S. Svanberg, and K. Svanberg, "Interstitial photodynamic therapy—diagnostic measurements and treatment in malignant experimental rat tumours," in *Optical Biopsy and Tissue Optics*, I. J. Bigio, G. J. Mueller, G. J. Puppels, R. W. Steiner, and K. Svanberg, eds., Proc. SPIE **4161,** 151–157 (2000).
17. M. Soto Thompson, T. Johansson, S. Pålsson, S. Andersson-Engels, S. Svanberg, N. Bendsoe, U. Stenram, K. Svanberg, J. Spigulis, A. Derjabo, and J. Kapostins are preparing a manuscript to be called "Photodynamic therapy of basal cell carcinoma with multi-fibre contact light delivery."
18. C. af Klinteberg, M. Andreasson, O. Sandström, S. Andersson-Engels, and S. Svanberg, "Compact medical fluorosensor for minimally invasive tissue characterization," Rev. Sci. Instrum. **76,** 034303-1 (2005).
19. U. Gustafsson, S. Pålsson, and S. Svanberg, "Compact fibre-optic fluorosensor using a continuous wave violet diode laser and an integrated spectrometer," Rev. Sci. Instrum. **71,** 3004–3006 (2000).
20. S. Svanberg, S. Andersson-Engels, and K. Svanberg, "Divider for distributing radiation," Swedish patent SE 503 408 (14 November 2001).
21. K. M. Case and P. F. Zweifel, *Linear Transport Theory* (Addison-Wesley, 1967).
22. J. B. Fishkin, O. Coquoz, E. R. Anderson, M. Brenner, and B. J. Tromberg, "Frequency-domain photon migration measurements of normal and malignant tissue optical properties in a human subject," Appl. Opt. **36,** 10–20 (1997).
23. A. J. Welch and M. J. C. van Gemert, *Optical-Thermal Response of Laser-Irradiated Tissue* (Plenum, 1995).
24. K. König, H. Schneckenburger, A. Rück, and R. Steiner, "*In vivo* photoproduct formation during PDT with ALA-induced endogenous porphyrins," J. Photochem. Photobiol. B. **18,** 287–290 (1993).
25. S. A. Prahl, "Tabulated molar extinction coefficient for hemoglobin in water," Oregon Medical Laser Center (1998), omlc.ogi.edu/spectra/hemoglobin/summary.html.
26. R. M. P. Doornbos, R. Lang, M. C. Aalders, F. W. Cross, and H. J. C. M. Sterenborg, "The determination of *in vivo* human tissue optical properties and absolute chromophore concentrations using spatially resolved steady-state diffuse reflectance spectroscopy," Phys. Med. Biol. **44,** 967–981 (1999).
27. D. J. Robinson, H. S. de Bruijn, N. van der Veen, M. R. Stringer, S. B. Brown, and W. M. Star, "Protoporphyrin IX fluorescence photobleaching during ALA-mediated photodynamic therapy of UVB-induced tumors in hairless mouse skin," Photochem. Photobiol. **69,** 61–70 (1999).
28. M. Soumya and T. H. Foster, "Carbogen breathing significantly enhances the penetration of red light in murine tumours *in vivo*," Phys. Med. Biol. **49,** 1891–1904 (2004).
29. D. J. Robinson, H. S. de Bruijn, N. van der Veen, M. R. Stringer, S. B. Brown, and W. M. Star, "Fluorescence photobleaching of ALA-induced protoporphyrin IX during photodynamic therapy of normal hairless mouse skin: the effect of light dose and irradiance and the resulting biological effect," Photochem. Photobiol. **67,** 140–149 (1998).
30. Q. Chen, B. C. Wilson, S. D. Shetty, M. S. Patterson, J. C. Cerny, and F. W. Hetzel, "Changes in *in vivo* optical properties and light distributions in normal canine prostate during photodynamic therapy," Radiat. Res. **147,** 86–91 (1997).
31. A. M. K. Nilsson, R. Berg, and S. Andersson-Engels, "Measurements of the optical properties of tissue in conjunction with photodynamic therapy," Appl. Opt. **34,** 4609–4619 (1995).
32. J. P. A. Marijnissen and W. M. Star, "Quantitative light dosimetry in vitro and *in vivo*," Lasers Med. Sci. **2,** 235–242 (1987).
33. A. Johansson, T. Johansson, M. Soto Thompson, N. Bendsoe, K. Svanberg, S. Svanberg, and S. Andersson-Engels are preparing a manuscript to be called "*In vivo* measurement of parameters of dosimetric importance during photodynamic therapy of thick skin tumors."
34. I. A. Boere, D. J. Robinson, H. S. de Bruijn, J. van den Boogert, H. W. Tilanus, H. J. C. M. Sterenborg, and R. W. F. de Bruin, "Monitoring in situ dosimetry and protoporphyrin IX fluorescence photobleaching in the normal rat esophagus during 5-aminolevulinic acid photodynamic therapy," Photochem. Photobiol. **78,** 271–272 (2003).
35. F. B. Jensen, "Red blood cell pH, the Bohr effect, and other oxygenation-linked phenomena in blood O_2 and CO_2 transport," Acta Phys. Scand. **182,** 215–227 (2004).
36. A. Curnow, J. C. Haller, and S. G. Bown, "Oxygen monitoring during 5-aminolaevulinic acid induced photodynamic therapy in normal rat colon. Comparison of continuous and fractionated light regimes," J. Photochem. Photobiol. B. **58,** 149–155 (2000).
37. J. H. Woodhams, L. Kunz, S. G. Bown, and A. J. MacRobert, "Correlation of real-time haemoglobin oxygen saturation monitoring during photodynamic therapy with microvascular effects and tissue necrosis in normal rat liver," Br. J. Cancer **91,** 788–794 (2004).
38. Q. Chen, Z. Huang, H. Chen, and H. Shapiro, "Improvement of tumour response by manipulation of tumour oxygenation during PDT," Photochem. Photobiol. **76,** 197–203 (2002).
39. D. R. Holmes, B. J. Davis, C. J. Bruce, and R. A. Robb, "3D

visualization, analysis, and treatment of the prostate using trans-urethral ultrasound," Comput. Med. Imaging Graph. **27,** 339–349 (2003).
40. L. K. Lee, C. Whitehurst, M. L. Pantelides, and J. V. Moore, "An interstitial light assembly for photodynamic therapy in prostatic carcinoma," Br. J. Urol. Int. **84,** 821–826 (1999).
41. A. Curnow, B. W. McIlroy, M. J. Postle-Hacon, A. J. MacRobert, and S. G. Bown, "Light dose fractionation to enhance photodynamic therapy using 5-aminolevulinic acid in the normal rat colon," Photochem. Photobiol. **69,** 71–76 (1999).
42. S. R. Arridge, "Optical tomography in medical imaging," Inverse Probl. **15,** R41–R93 (1999).